Long-Range Single-Baseline RTK for Complementing Network-Based RTK

Don Kim and Richard B. Langley

Geodetic Research Laboratory, Department of Geodesy and Geomatics Engineering
University of New Brunswick, Fredericton, New Brunswick, Canada

BIOGRAPHY

Don Kim is a senior research associate in the Department of Geodesy and Geomatics Engineering at the University of New Brunswick (UNB). He has a bachelor's degree in urban engineering, and M.Sc.E. and Ph.D. in geomatics from Seoul National University. He has been involved in GPS research since 1991 and active in the development of an ultrahigh-performance RTK system. He received the Dr. Samuel M. Burka Award for 2003 from The Institute of Navigation (ION).

Richard B. Langley is a professor in the Department of Geodesy and Geomatics Engineering at UNB, where he has been teaching since 1981. He has a B.Sc. in applied physics from the University of Waterloo and a Ph.D. in experimental space science from York University, Toronto. Prof. Langley has been active in the development of GPS error models since the early 1980s and is a contributing editor and columnist for GPS World magazine. He is a fellow of the ION and the Royal Institute of Navigation and shared the ION 2003 Burka Award with Don Kim.

ABSTRACT

One of the major challenges in resolving ambiguities for longer baselines is the presence of unmodelled ionospheric and tropospheric delays. In this paper, we describe a new approach that does not rely on the convergence of atmospheric parameters. The new approach instantaneously nullifies the effect of the differential ionospheric delay in an ambiguity search process and simultaneously estimates the differential tropospheric delay and baseline components at every epoch.

The performance of the new approach was demonstrated using the data recorded at a 1 Hz data rate at a pair of base stations on either side of the Bay of Fundy in eastern Canada and on a ferry boat, at the terminals of an approximately 74 km ferry route, on 21 May 2004. For both static and kinematic tests over the longer 74 km baseline, mean differences of a few millimetres were observed in each Cartesian component, and the comparison 1σ noise level was at the few centimetre level.

INTRODUCTION

Biases and errors such as satellite orbit error and atmospheric (i.e., tropospheric and ionospheric) signal refraction are the primary limiting factors in successful long-baseline, real-time kinematic (RTK) style processing – either in real-time or post-processing mode. These error sources are dependent on the distance between a reference and a rover receiver. If they are not adequately accounted for, they can result in significant positioning errors in long-baseline applications. This is particularly true for the conventional single-baseline RTK and hence reduces the effective inter-receiver distance of this technique to a few 10s of km.

There are effective mitigation strategies for these error sources. For example, the ionosphere-free linear combination of the L1 and L2 carrier-phase measurements can completely cancel first-order ionospheric delays. Although this appeals in mitigating the ionospheric errors, we have to be prepared to accept some costs for that. As it is difficult to fix integer ambiguities using the ionosphere-free observations for long-baselines, float ambiguity solutions (less accurate than fixed ones) are normally used. Due to the amplification of the noise by the combination, the solutions are less precise, too. Errors in broadcast GPS satellite orbits have little effect for baselines up to a few 100 km and furthermore, can be virtually eliminated using precise ephemerides in post-processing mode. Tropospheric delay is usually estimated based on model atmospheric predictions and/or surface meteorological observations made near the stations at the time of the GPS measurements. As this approach often inappropriately accounts for spatial and temporal variations in water vapor delays [Brunner and Welsch , 1993; Niell et al., 2001], it is a common procedure to estimate a residual zenith delay.

As an alternative approach to mitigating the error sources, network RTK based on multiple reference stations is used [Wubbena et al., 2001; Landau et al., 2002; Rizos, 2002; Fotopoulos and Cannon, 2001; Kashani et al., 2004]. The integration of several reference stations into a combined network provides a capability for modeling the error sources at a rover within the network and enables lengthening the baselines up to a few 100s of km. Despite successful implementation of network RTK for long-baseline applications, however, its performance is not always equivalent to single-baseline RTK operating under short-baseline situations. As network RTK interpolates error corrections for a rover using the error estimates at reference stations, this approach is vulnerable to localized anomalous errors under unfavorable atmospheric conditions. For example, weather fronts and atmospheric conditions associated with heavy rainfall can cause rapid variations in the tropospheric delay [Gregorius and Blewitt, 1998] and subsequently, the performance of an RTK system can be significantly degraded even across relatively short baselines [Skidmore and Van Graas, 2004; Lawrence et al., 2006]. Such anomalies are not canceled in the interpolation procedure used for deriving rover delays. Also, solar-terrestrial interactions can cause significant changes in the morphology of the ionosphere, changing the propagation delay of GPS signals within time intervals as short as one minute. Such changes can last for several hours primarily in the polar, auroral and equatorial ionospheres [Langley, 2000]. During severe ionospheric activity, the correction accuracy deteriorates and adversely affects the ambiguity resolution over the network [Wielgosz et al, 2005; Petrovski et al., 2002]. When a rover is located outside the network boundary, network RTK must extrapolate error corrections for the rover. As a result, network RTK can face the same challenges as single-baseline RTK.

Over the past a few years, the University of New Brunswick (UNB) has carried out several research projects involving long baselines that, unfortunately, could not take advantage of network RTK. These include a field experiment to investigate the performance of different neutral atmosphere mitigation strategies during the 2005 mission of the Canadian Coast Guard Ship Amundsen (a research icebreaker) in the Canadian Arctic and Hudson Bay [Ghoddousi-Fard and Dare, 2006], and collaboration with the University of Southern Mississippi to advance positioning results by means of improved differential tropospheric modeling in the marine environment of the Bay of Fundy in eastern Canada [Kim et al., 2004]. In both studies, the number of reference stations deployed was not sufficient to adequately model the errors using network RTK. Instead, our approach for achieving high accuracies at greater distances from differential reference stations was single-baseline RTK in post-processing mode.

In this paper, we describe an UNB approach for long-range RTK. Although this approach was originally developed for single-baseline RTK over long distances in kinematic mode, it can be used for network RTK when requiring extrapolation of the differential ionosphere corrections for a rover located outside the network. It can also be used in cases where the rover located inside the network is experiencing local anomalies in the differential ionospheric delays.

CONSIDERATIONS FOR A NEW APPROACH

The most common approach for achieving high accuracies with GPS technology in kinematic situations is RTK-style processing. On designing an appropriate approach for long-range (e.g., 30-100 km) single-baseline RTK, we consider two basic requirements. Firstly, our new approach will be used in real-time applications such as machine guidance and vehicle navigation. More specifically, single epoch carrier-phase observations will be used to resolve ambiguities (that is, an epoch-by-epoch ambiguity resolution) in real-time situations. Secondly, the new approach will provide positioning solutions using fixed ambiguities rather than the ionosphere-free float ambiguities.

The Observation Model

The DD (double-differenced between satellites and receivers) carrier-phase observations are used in our approach. The linearized GPS carrier-phase observation model for long-range single-baseline applications is given as:

$$\mathbf{y}_i = \mathbf{A}\mathbf{x} + \mathbf{s} + \mathbf{T} - \mathbf{I}_i + \lambda_i \mathbf{N}_i + \mathbf{e}_i, \quad Cov[\mathbf{e}_i] = \mathbf{Q}_{\mathbf{y}_i}, \quad i = 1 \text{ or } 2, \tag{1}$$

where $\mathbf{y}$ is the vector of DD carrier-phase in distance units; $\mathbf{x}$ is the vector of unknown baseline components; $\mathbf{s}$ is the vector of orbit error contributions to the DD carrier-phase observations; $\mathbf{T}$ is the vector of DD tropospheric delays; $\mathbf{I}$ is the DD ionospheric delay parameter vector where $\mathbf{I}_2 = \left(f_{L1}^2 / f_{L2}^2\right)\mathbf{I}_1$; $\mathbf{A}$ is the design matrix corresponding to $\mathbf{x}$; $\mathbf{N}$ is the vector of DD ambiguities; f and λ are the frequency and wavelength of the carrier-phase observations, respectively; $\mathbf{e}$ is the noise vector including multipath, residual ionospheric delay (e.g., higher-order ionospheric effects [Bassiri and Hajj, 1993; Hoque and Jakowski, 2007] and ionospheric scintillation [Langley, 2000]) and receiver system noise; $Cov[\cdot]$ represents the variance-covariance operator; $\mathbf{Q}_{\mathbf{y}}$ is the variance-covariance matrix of the observations; and i indicates the L1 or L2 signal.

The Objective Function

Least-squares estimation with integer constraint for the ambiguity parameters is referred to as an integer least-squares problem. The objective function to be minimized in the integer least-squares problem, Ω, is given as [Euler and Landau, 1992; Teunissen, 1995]:

$$\Omega_i = \left(\hat{\mathbf{N}}_i - \breve{\mathbf{N}}_i\right)^{\mathrm{T}} \mathbf{Q}_{\hat{\mathbf{N}}_i}^{-1} \left(\hat{\mathbf{N}}_i - \breve{\mathbf{N}}_i\right), \quad with\ \breve{\mathbf{N}}_i \in \mathbb{Z}^n, \quad i = 1 \text{ or } 2, \tag{2}$$

where $\hat{\mathbf{N}}$ is the vector of float ambiguity estimates; $\breve{\mathbf{N}}$ is the vector of integer ambiguity candidates selected in the ambiguity search process; $\mathbf{Q}_{\hat{\mathbf{N}}}$ is the variance-covariance matrix of the float ambiguity estimates; $\mathbb{Z}$ is the set of integers; n is the number of the observations; and, again, i indicates the L1 or L2 signal.

Satellite Orbit Errors

Errors in broadcast GPS satellite orbits have little effect for baselines up to a few 100 km and furthermore, can be virtually eliminated using precise ephemerides in post-processing mode. Using the well-known "rule of thumb" validated using International GNSS Service (IGS) data, an approximate baseline component error becomes around 2 cm over a baseline of 100 km with around 4 m orbital error [Beutler, 1998; Ziebart et al., 2002].

Broadcast Orbits The errors of the broadcast orbits can be statistically quantified by comparing the broadcast orbits with the IGS Final or IGS Rapid product. The IGS rapid products have a quality comparable to that of the final products. Figure 1 shows the weighted r.m.s. errors of the broadcast orbits with respect to the IGS rapid product [IGS GFZ, 2007]. We also do an automated daily analysis on the broadcast orbits at UNB [UNB GGE, 2007]. As illustrated in Figure 1, the weighted r.m.s. errors of the broadcast orbits are currently much smaller than 4 m, which may result in smaller than 2 cm baseline component errors over a baseline of 100 km. As the effects of the broadcast orbit errors are not significant for a baseline of up to 100 km, therefore, we can safely ignore the orbit error term $\mathbf{s}$ in Eq. (1) when using the broadcast orbits in real-time applications.

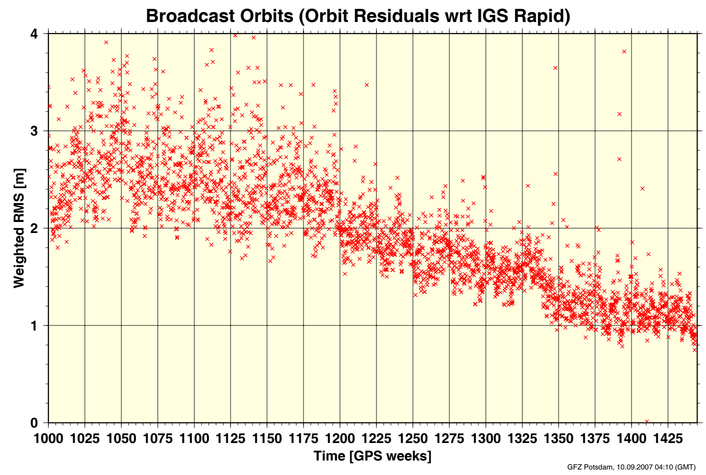

Figure 1. broadcast orbit errors compared with the IGS Rapid product, created by the IGS Analysis Center Coordinator at GFZ (GeoForschungsZentrum) Potsdam.

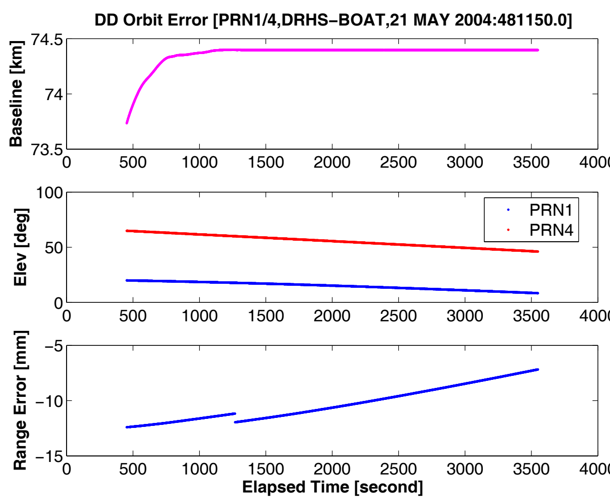

Figure 2. Double-differenced broadcast orbit errors based on a comparison with the NGA APC precise ephemeris for the long baselines, projected onto the range direction.

NGA Precise Orbits The National Geospatial-intelligence Agency (NGA) provides precise GPS ephemeris files referenced to satellite antenna phase center (APC) rather than center of mass. Figure 2 shows an example of double-differenced broadcast orbit errors compared to the NGA APC precise ephemeris for long baselines. These orbit errors were projected onto the range direction. The top panel shows the distances (about 74 km) between a base station and a rover, the middle panel shows the elevation angles of the paired satellites used in double differencing, and the bottom panel shows the broadcast orbit errors in the range direction. The jump in the range error plot is due to a switch in two-hour broadcast ephemeris sets. It is obvious that range error differences using the broadcast orbit can reach up to a few cm for the long baselines. Compared to the wavelength of the carrier-phase observations, however, range errors due to the broadcast orbits are not significant. This confirms that we can safely ignore the orbit error term **s** in Eq. (1) when using the broadcast orbits in real-time applications over a baseline of up to 100 km.

Ionospheric Delays

The ionosphere-free linear combination and ionosphere modeling as a state work well for long baselines once the parameter (i.e., ionospheric delay or float ambiguities) converges although it takes typically a few hours. In real-time applications requiring millimetre accuracy, however, these approaches are not practical. Instead, we use the ionosphere-nullification technique [Kim and Langley, 2005] that instantaneously nullifies the effect of the differential ionospheric delay in an ambiguity search process.

The Ionosphere Observable In the ionosphere-nullification technique, the ionospheric delay can be derived from the geometry-free combination (that is, the difference of L1 and L2 carrier-phase observations in distance units) once the L1 and L2 ambiguity parameters are given as known values. The L1 and L2 ionosphere observables are given as:

$$\begin{aligned}\hat{\mathbf{I}}_1 &= \left(\frac{f_{L2}^2}{f_{L1}^2 - f_{L2}^2}\right)\left[\mathbf{y}_1 - \mathbf{y}_2 - \left(\lambda_1 \breve{\mathbf{N}}_1 - \lambda_2 \breve{\mathbf{N}}_2\right)\right] \\ \hat{\mathbf{I}}_2 &= \left(\frac{f_{L1}^2}{f_{L2}^2}\right)\hat{\mathbf{I}}_1,\end{aligned} \tag{3}$$

where again, $\breve{\mathbf{N}}$ is the vector of integer ambiguity candidates selected in the ambiguity search process. As the tropospheric delay and satellite orbit error do not depend on the signal frequency, they are completely eliminated by differencing the L1 and L2 carrier-phase observations in Eq. (3). Therefore, these two error sources are irrelevant to the ionosphere observable. This aspect of the ionosphere observable enables us to isolate the ionospheric delay from the tropospheric delay and satellite orbit error in long-baseline situations and to evaluate its effects on the performance of long-range RTK.

Ionosphere Nullification It is assumed in the ionosphere-nullification technique that we can combine the two independent L1 and L2 ambiguity search processes into one simultaneous ambiguity search process. When a pair of L1 and L2 ambiguity candidates is selected in the simultaneous ambiguity search process, we can virtually eliminate the large residual ionospheric effects (i.e., the first-order differential ionospheric delays) using the ionosphere observable in Eq. (3). Furthermore, this approach is able to instantaneously eliminate the differential ionospheric delay.

As the ionosphere-nullification technique estimates the ionospheric delays and ambiguities simultaneously using single epoch carrier-phase observations (that is, an epoch-by-epoch ambiguity resolution), this technique may be less reliable than alternatives which model the ionospheric delays as a state in a Kalman filter or a sequential least-squares estimator. This is more likely to be true especially when the number of satellites being observed is insufficient (e.g., less than or equal to 6 satellites). However, under a typical condition (e.g., more than 6 satellites), the performance of the ionosphere-nullification technique is comparable to the alternatives.

Tropospheric Delays

In precise applications requiring millimetre accuracy, the tropospheric delay can be estimated by a simple parameterization of the tropospheric delay. The line of sight delay D is expressed as a function of four parameters as follows [McCarthy and Petit, 2003]:

$$D = m_h\left(el\right)D_{hz} + m_w\left(el\right)D_{wz} + m_g\left(el\right)\left[G_N\cos\left(az\right) + G_E\sin\left(az\right)\right] \tag{4}$$

where D_{hz} is the zenith hydrostatic delay; D_{wz} is the zenith non-hydrostatic or wet delay; G_N and G_E are the north and east delay gradient in distance units, respectively; m_h, m_w and m_g are the hydrostatic, wet and gradient mapping functions, respectively; el is the non-refracted elevation angle at which the signal is received; and az is the azimuth angle at which the signal is received, measured east of north.

Under typical atmospheric conditions, GPS data may not have the sensitivity to detect atmospheric gradients and azimuthal asymmetry as included in Eq. (4). In such a case, the tropospheric delay can be estimated by restricting the residual error to the zenith delay components, such that:

$$D = m_h\left(el\right)D_{hz} + m_w\left(el\right)D_{wz}\,. \tag{5}$$

Hydrostatic Delay For the most accurate a priori hydrostatic delay, the formula of Saastamoinen [1972] as given by Davis et al. [1985] is used in this paper as:

$$D_{hz} = \frac{\left(0.0022768 \pm 0.0000005\right)P_0}{1 - 0.00266\left(\cos 2\phi\right) - 0.00028H}\,, \tag{6}$$

where P_0 is total atmospheric pressure in millibars at the antenna reference point; ϕ is the geodetic latitude of the site; and H is the height above the geoid (km).

Mapping Functions For the hydrostatic and wet mapping functions, Niell's NMF (New Mapping Functions) [Niell, 1996] are used in this paper. The NMF adopts the same form of Herring [1992] as:

$$f(el,a,b,c)=\frac{1+\cfrac{a}{1+\cfrac{b}{1+c}}}{\sin(el)+\cfrac{a}{\sin(el)+\cfrac{b}{\sin(el)+c}}}, \tag{7}$$

In the NMF, unlike the Herring model, the hydrostatic mapping function is dependent on latitude, season (i.e., day of the year) and the height above the geoid of the point of observation while the wet mapping function is dependent on latitude only. The NMF are given by

$$\begin{aligned} m_h(el) &= f_h(el,a,b,c)+\left[\frac{1}{\sin(el)}-f_{ht}(el,a,b,c)\right]H \\ m_w(el) &= f_w(el,a,b,c), \end{aligned} \tag{8}$$

where again, *el* is the elevation angle at which the signal is received; H is the height above the geoid (km); and subscripts *h*, *w* and *ht* indicate that the function *f* uses the coefficients *a*, *b* and *c* corresponding to the hydrostatic and wet mapping functions and height correction, respectively.

For the gradient mapping function, Chen and Herring [1997] is used in this paper as:

$$\mathrm{m_g}(el)=\frac{1}{\sin(el)\tan(el)+0.0032}. \tag{9}$$

ESTIMATION MODEL

Assuming that accurate real-time meteorological data are available at a reference station and a rover, we can use Eq. (6) to remove the hydrostatic delay in Eq. (4) or (5). To avoid a mathematical correlation between the partial derivatives of the tropospheric delay at two stations, the levering technique [Rocken et al., 1995] can be used, which fixes the tropospheric delay at the reference station and estimate the relative delay at the rover. Then, from Eq. (4) or (5), the DD tropospheric delay T is given by

$$T_{AB}^{uv}=SD_B^{uv}(D)-SD_A^{uv}(D)=mD+\mathbf{m\tau}, \tag{10}$$

where $SD(\cdot)$ is the single-difference (between satellites *u* and *v*) operator; subscripts A and B indicate a reference station and a rover, respectively; and

$$\begin{aligned} mD &= SD_B^{uv}(m_h D_{hz})-SD_A^{uv}(m_h D_{hz}) \\ \mathbf{m} &= \left[SD_B^{uv}(m_w) \quad SD_B^{uv}(m_g\cos(az)) \quad SD_B^{uv}(m_g\sin(az))\right] \\ \boldsymbol{\tau} &= \left[D_{wz} \quad G_N \quad G_E\right]^T. \end{aligned} \tag{11}$$

By substituting Eqs. (10) and (11) into Eq. (1), and ignoring the orbit error term **s** in Eq. (1), we will have a new carrier-phase observation model for long-range single-baseline applications as:

$$\mathbf{y}_i'=\mathbf{Bz}-\mathbf{I}_i+\lambda_i\mathbf{N}_i+\mathbf{e}_i', \quad Cov[\mathbf{e}_i']=\mathbf{Q}_{\mathbf{y}'_i}, \quad i=1 \text{ or } 2, \tag{12}$$

where

$$\mathbf{y}_i'=\mathbf{y}_i-\mathbf{mD}, \quad \mathbf{B}=[\mathbf{A} \quad \mathbf{M}], \quad \mathbf{z}=[\mathbf{x}^T \quad \boldsymbol{\tau}^T]^T \tag{13}$$

and $\mathbf{mD}=\left[mD_1 \ \cdots \ mD_n\right]^T$; $\mathbf{M}=\left[\mathbf{m}_1^T \ \cdots \ \mathbf{m}_n^T\right]^T$; and n is the number of DD carrier-phase observations. Note that the new carrier-phase observation model in Eq. (12) can be used to estimate the unknown parameters (i.e., the baseline components $\mathbf{x}$, the tropospheric delay $\boldsymbol{\tau}$) at every epoch. The ionospheric delay $\mathbf{I}$ and ambiguities $\mathbf{N}$ are resolved in the ambiguity search process using the ionosphere nullification technique.

Adaptive Estimator

Since the tropospheric delays will not change dramatically under a typical atmospheric condition over a short time period, it might be better to estimate adaptively the tropospheric delay parameter as:

$$\bar{\boldsymbol{\tau}}_k=\alpha\hat{\boldsymbol{\tau}}_k+(1-\alpha)\bar{\boldsymbol{\tau}}_{k-1}, \quad 0<\alpha\le 1, \tag{14}$$

where $\hat{\boldsymbol{\tau}}_k$ is the estimate of the tropospheric delay parameter at epoch *k*; $\bar{\boldsymbol{\tau}}_k$ is the adaptive estimate of $\hat{\boldsymbol{\tau}}_k$; and α is a forgetting factor which is reciprocal to a correlation time (i.e., a smoothing time interval). Depending on an atmospheric condition, we can control the correlation time of the tropospheric delay parameter by changing α. Substituting $\hat{\boldsymbol{\tau}}_k$ into Eq. (12) gives

$$\mathbf{y}_{i,k}''=\mathbf{B}_k'\mathbf{z}_k'-\mathbf{I}_{i,k}+\lambda_i\mathbf{N}_{i,k}+\mathbf{e}_{i,k}'', \quad Cov\left[\mathbf{e}_{i,k}''\right]=\mathbf{Q}_{\mathbf{y}''_{i,k}}, \quad i=1 \text{ or } 2 \tag{15}$$

where

$$
\begin{aligned}
\mathbf{y}''_{i,k} &= \mathbf{y}'_{i,k} + \frac{1-\alpha}{\alpha}\mathbf{M}_k \overline{\boldsymbol{\tau}}_{k-1} \\
\mathbf{B}'_k &= \begin{bmatrix} \mathbf{A}_k & \dfrac{1}{\alpha}\mathbf{M}_k \end{bmatrix}, \quad \mathbf{z}'_k = \begin{bmatrix} \mathbf{x}_k^T & \overline{\boldsymbol{\tau}}_k^T \end{bmatrix}^T
\end{aligned}
\tag{16}
$$

Finally, Eq. (15) can be initialized using $\overline{\boldsymbol{\tau}}_0 = \hat{\boldsymbol{\tau}}_0$ where $\hat{\boldsymbol{\tau}}_0$ is an estimate of the tropospheric delay parameter at an initial epoch. It should be noted that the ionosphere observable in Eq. (3) will not be changed by this carrier-phase observation model. We use this observation model in our approach for real-time applications.

The Ionosphere-Nullification Approach

Assuming that a simultaneous search process for L1 and L2 ambiguity parameters has been established, a pair of L1 and L2 ambiguity candidates can be selected in the process. Then, we can derive the L1 and L2 ionosphere observables in Eq. (3) using the ambiguity candidates. As a matter of fact, each ambiguity candidate provides its corresponding ionosphere observation. Once we have a new ionosphere observation, we can estimate a new float ambiguity estimate, $\hat{\mathbf{N}}_i$, as given in Figure 3. This new float ambiguity estimate is virtually free from the effects of the ionospheric delay. It should be noted that the updated variance-covariance matrix, $\mathbf{Q}_{\hat{\mathbf{N}}_i} (= \mathbf{Q}_{\hat{\mathbf{N}}_{i0}, \hat{\mathbf{I}}_i})$, as well as the float solutions, $\hat{\mathbf{N}}_{i0}$ and $\mathbf{Q}_{\hat{\mathbf{N}}_{i0}}$, are computed once for every epoch's observations outside the ambiguity search space. We have to carry out the same procedure on each candidate sequentially until no ambiguity candidate remains. Then, our goal is to find the ambiguity candidate that minimizes the objective function in Eq. (2). Figure 3 shows the ionosphere-nullification procedure.

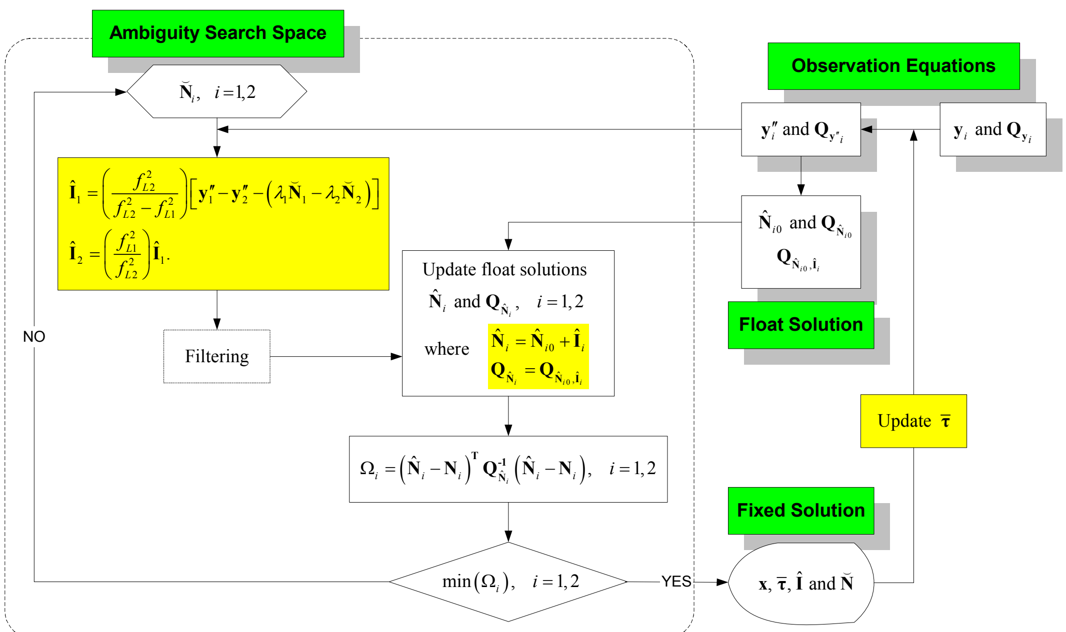

Figure 3. Ionosphere-nullification procedure incorporated in the ambiguity search process for long-range single-baseline RTK applications.

One issue involved with the ionosphere-nullification technique is that the ionosphere observables in Eq. (3) are apt to be affected by multipath, receiver system noise and residual ionospheric delay. As tropospheric delay and satellite orbit error are eliminated, they are irrelevant to the ionosphere observables. From Eq. (3), the noise terms of the ionosphere observables become

$$
\begin{aligned}
\boldsymbol{\varepsilon}(\hat{\mathbf{I}}_1) &= \left(\frac{f_{L2}^2}{f_{L1}^2 - f_{L2}^2}\right)\left[\tilde{\mathbf{e}}_1 - \tilde{\mathbf{e}}_2 + \mathbf{m}_1 - \mathbf{m}_2\right] \\
\boldsymbol{\varepsilon}(\hat{\mathbf{I}}_2) &= \left(\frac{f_{L1}^2}{f_{L2}^2}\right)\boldsymbol{\varepsilon}(\hat{\mathbf{I}}_1),
\end{aligned}
\tag{17}
$$

where $\boldsymbol{\varepsilon}(\cdot)$ denotes the noise associated with the ionosphere observable and $\tilde{\mathbf{e}}$ represents the noise vector without residual orbit error and residual tropospheric delay. It should be noted that multipath is normally a dominant error source in the ionosphere observables. So ideally, a GPS antenna should be installed in a clear place with no close-by reflector in the vicinity of the antenna if the ionosphere-nullification technique is to be used in RTK processing. Otherwise, we need to reduce the effects of multipath in the carrier-phase observations when we process the data. The 'Filtering' block in Figure 3 can be designed to help take care of this issue.

TEST RESULTS

Two GPS reference stations had been deployed at the Canadian Coast Guard building in Saint John, New Brunswick (CGSJ) and at the Digby Regional High School in Digby, Nova Scotia (DRHS), on either side of the Bay of Fundy, near the terminals of an approximately 74 km marine ferry route (see Figure 4). Two geodetic-grade receivers (NovAtel's DL-4 receivers and GPS-600 antennas) had been installed at the reference stations. Also, the same type of receiver had been installed on the ferry – the Princess of Acadia. Surface meteorological equipment had also been collocated with the three receivers. This ferry repeats the same routes between two and four times daily, depending upon the season. The Bay of Fundy is located in a temperate climate region with significant seasonal tropospheric variations (e.g., temperatures between -30°C and +30°C). Data had been collected over the course of one year from the daily ferry runs.

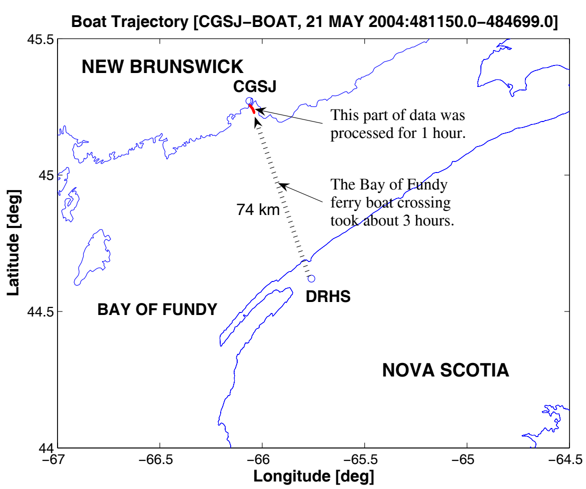

Figure 4. Test data for comparing long/short baselines to the same rover.

Using the UNB RTK software, we post-processed the data recorded at a 1 Hz data rate at the pair of base stations (CGSJ and DRHS) and the ferry boat on 21 May 2004. We used a zero elevation cutoff angle for data processing. One of the tools we use to assess the success of atmospheric modeling or other approaches such as the ionosphere-nullification technique, is the comparison between short baseline (e.g., less than a few 10s of km) RTK solutions (for which RTK is generally regarded as reliable and uncontaminated by differential atmospheric uncertainties) and simultaneous position solutions from longer RTK baselines over which the atmospheric models or other approaches are being assessed. As we intended to compare long/short baselines to the same rover to characterize long-baseline positioning performance, we processed a subset of the data near the end of a ferry run that provides such long/short baselines. Figure 4 illustrates the ferry crossing from Digby to Saint John and the data subset used. This situation provided both short (< 3 km) and long (> 73 km) baselines at the same time for one hour.

Ionosphere Nullification

The DD ionospheric delays in Figure 5 are epoch-by-epoch estimates obtained by the ionosphere-nullification technique incorporated in the ambiguity resolution process. How do we know that the ionospheric delays in the L1 and L2 carrier-phase measurements are eliminated by the ionosphere-nullification technique? We can confirm this by examining the residual error in each observation. From Eq. (15), the ionosphere-nullified observations are given as:

$$\mathbf{y}_{1,IF} = \mathbf{y}_1'' + \hat{\mathbf{I}}_1, \quad \mathbf{y}_{2,IF} = \mathbf{y}_2'' + \hat{\mathbf{I}}_2, \quad \mathbf{y}_{IF} = \left(\frac{f_{L1}^2}{f_{L2}^2}\right)\mathbf{y}_1'' - \mathbf{y}_2'', \tag{18}$$

where $\mathbf{y}_{1,IF}$ and $\mathbf{y}_{2,IF}$ are the ionosphere-nullified L1 and L2 observations, respectively; and $\mathbf{y}_{IF}$ is the ionosphere-free linear combination. Then, the noise terms of the ionosphere-nullified observations become

$$\begin{aligned}\boldsymbol{\varepsilon}(\mathbf{y}_{1,IF}) &= \boldsymbol{\varepsilon}(\mathbf{y}_{2,IF}) = \boldsymbol{\varepsilon}(\mathbf{y}_{IF}) \\ &= \left(\frac{f_{L1}^2}{f_{L1}^2 - f_{L2}^2}\right)\mathbf{e}_1'' + \left(\frac{-f_{L2}^2}{f_{L1}^2 - f_{L2}^2}\right)\mathbf{e}_2''.\end{aligned} \tag{19}$$

All three observations have the same noise components in Eq. (19). Note that the ionosphere-nullified L1 and L2 noise terms include multipath, residual orbit error, residual tropospheric delay, residual ionospheric delay and receiver system noise contributions from both frequencies. The 'Filtering' block in Figure 3 can be designed to reduce the high-frequency components of these errors.

Figure 6 shows that the residuals of the L1 and L2 observations are almost identical to those of the ionosphere-free linear combinations. This implies that the effects of the ionospheric delays have been successfully nullified in the L1 and L2 observations. Minor differences in the residuals of the three observation types come from the noise models used for least-squares estimation. For simplicity, we did not propagate the uncertainty of the ionospheric delay estimates into the ionosphere-nullified L1 and L2 observations. The effects of this negligence are insignificant as seen in Figure 6.

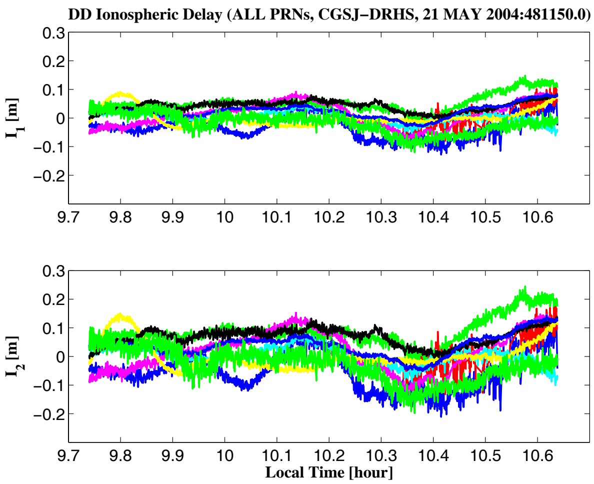

Figure 5. Double-differenced ionospheric delay estimates obtained by the ionosphere-nullification technique incorporated in ambiguity search process.

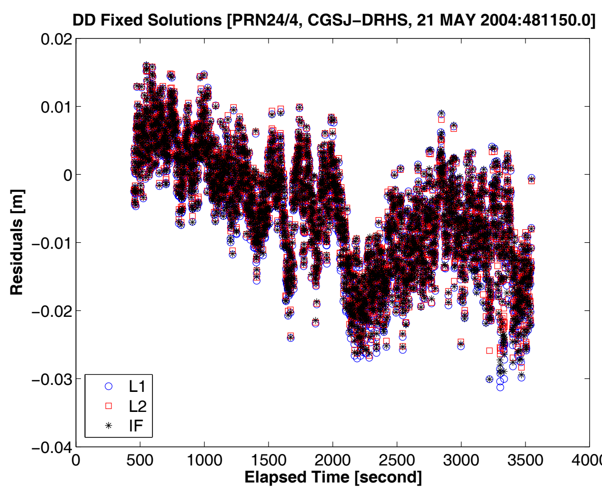

Figure 6. Residuals of the ionosphere-nullified observations after fixing ambiguities.

Estimation of the Tropospheric Delay

An unmodelled tropospheric zenith delay error causes an error in height determination. At very high elevation angles, an error in the tropospheric zenith delay is almost indistinguishable from the unmodelled height component. The zenith delay error can be well recovered at the low elevation angles, which can subsequently increase the error in height determination if not done correctly. These results can be improved if tight constraints are placed on the station height components in static applications [Collins and Langley, 1997].

On the other hand, the adaptive estimator represented by Eq. (15) can be used in kinematic applications as well as static applications. The adaptive estimator captures the changes of satellite geometry and mapping functions over a relatively short time period. This ability of the adaptive estimator enables us to distinguish the tropospheric zenith delay from the unmodelled height component. Figure 7 shows the condition number associated with $\mathbf{B}'_k$ in Eq. (16), which is defined by the ratio of maximal and minimal eigenvalues of $\mathbf{B}_k'^T \mathbf{B}'_k$. The condition number is a measure of how numerically well-conditioned or ill-conditioned the problem is. A lower condition number means that the tropospheric zenith delay is more distinguishable from the unmodelled height component. The top panel in Figure 7 shows the condition number for the single-epoch observation model in Eq. (12) while the middle panel is for the adaptive estimator. After around 2300 seconds in the elapsed time, the adaptive estimator converges to a low condition number while the single-epoch observation model does not. A sudden change of the condition number is due to the change of satellite constellation as illustrated in the bottom panel.

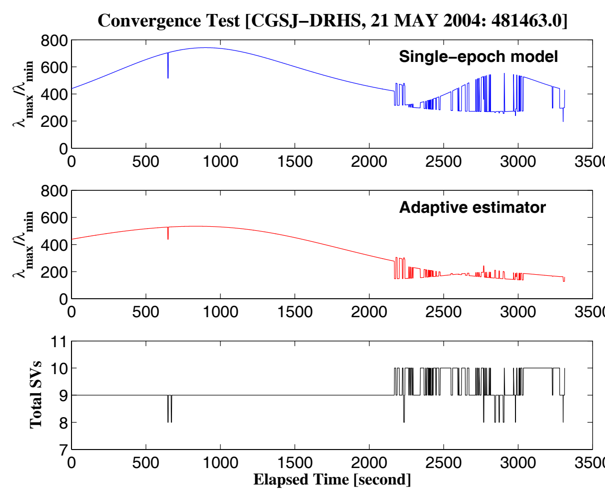

Figure 7. Condition numbers without atmospheric gradients and azimuthal asymmetry.

Figure 8 shows the wet zenith delay estimated at every epoch, without the assumption of atmospheric azimuthal asymmetry and use of gradient estimation. We can clearly see the effects of the forgetting factor α on the wet zenith delay estimates. When $\alpha = 1$, we obtain noisy wet zenith delay estimates as no smoothing process works on the estimates. On the other hand, we will have a smoother wet zenith delay estimate when α becomes smaller.

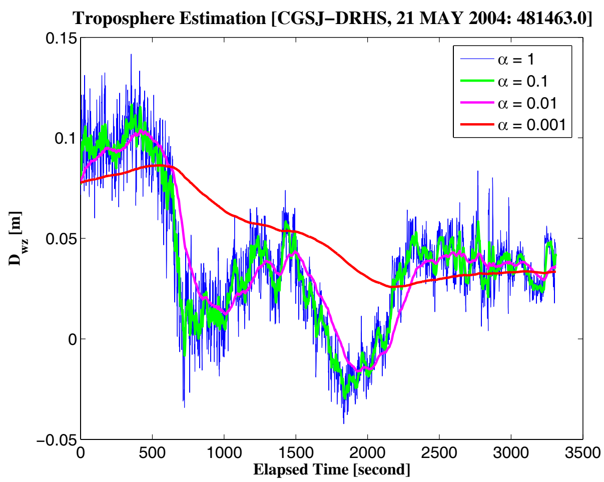

Figure 8. Effects of the forgetting factor α on the wet zenith delay estimates.

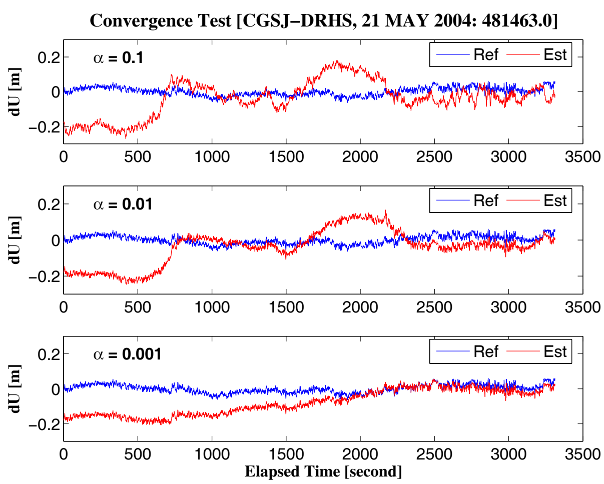

Figure 9. Convergence test of positioning solutions (vertical component) for different forgetting factors.

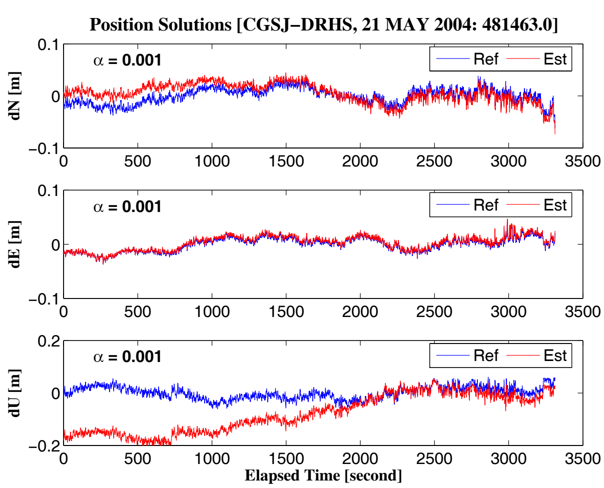

Figure 10. Convergence test of positioning solutions when $\alpha = 0.001$.

The convergence patterns of positioning solutions (vertical component) are illustrated in Figure 9. The reference solutions were determined by least-squares estimation after removing the atmospheric delays and ambiguities which can be estimated by fixing the coordinates of two reference stations, CGSJ and DRHS. Normally, a better performance of the adaptive estimator is anticipated for a smaller forgetting factor (i.e., a longer smoothing time interval) under typical atmospheric conditions. However, its performance may not be the same under severe atmospheric conditions. Figure 10 illustrates how well positioning solutions converge to the reference solutions when $\alpha = 0.001$.

We also tried to estimate the tropospheric delays with atmospheric gradients and azimuthal asymmetry. In this case, the tropospheric parameter vector includes the wet zenith delay D_{wz} and the horizontal (north G_N and east G_E) delay gradients. Figure 11 shows the tropospheric parameters estimated at every epoch when $\alpha = 0.001$. The zenith wet delay and the north delay gradient did not converge for a relatively long time period. It took about fifty minutes before they converged. Furthermore, as illustrated in Figure 12, positioning solutions were biased with respect to the reference solutions. The horizontal components (especially, the north solution) were more significantly biased than the vertical components.

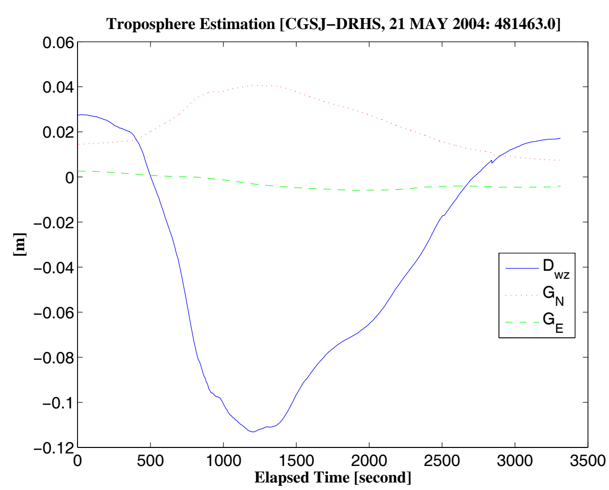

Figure 11. Estimates of the wet zenith delay and the horizontal delay gradient when $\alpha = 0.001$.

The condition numbers in Figure 13 explain why we had a poor performance with atmospheric gradients and azimuthal asymmetry. For both the single epoch observation model (top panel) and the adaptive estimator (middle panel), we had very high condition numbers. This means that the tropospheric parameters are almost indistinguishable from the unmodelled position components. To improve its performance, we may need a longer smoothing time interval or more satellites in lower elevation angles. Unfortunately, this may not be practical for real-time applications.

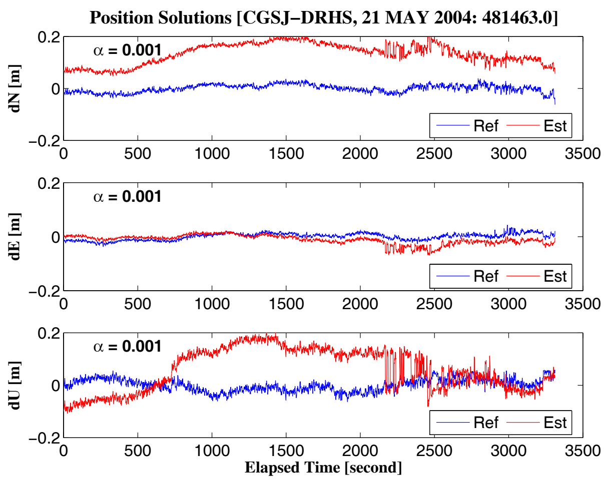

Figure 12. Convergence test of positioning solutions (horizontal and vertical components) when $\alpha = 0.001$.

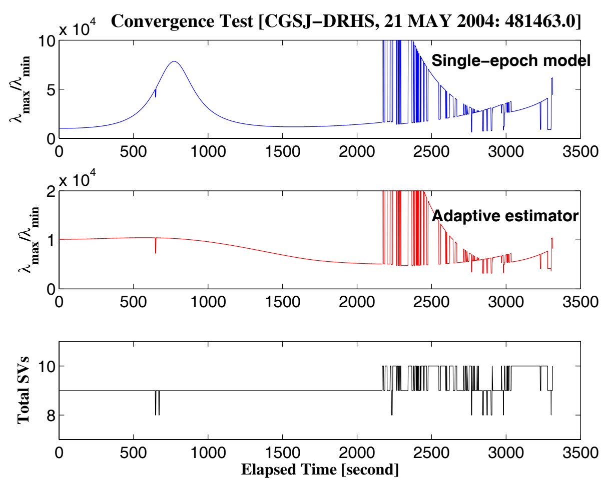

Figure 13. Condition numbers with atmospheric gradients and azimuthal asymmetry.

Static Results

A total of three permanent stations already in operation have been used to compute the geodetic coordinates of CGSJ and DRHS. One station is located in Fredericton, New Brunswick: the IGS station UNB1 (now UNBJ), on the UNB Fredericton campus. The other two stations are the U.S. CORS station ESPT, in Eastport, Maine, run by NOAA, and the IGS station HLFX, in Halifax, run by Natural Resources Canada. Seven days of raw GPS data from each of the five reference stations were processed with the Bernese V4.2 software [Hugentobler et al., 2001]. During the processing, the IGS final SP3 orbit product was used and the coordinates of all three permanent stations were held fixed to their published ITRF00 coordinates to estimate the coordinates of CGSJ and DRHS. The formal estimated uncertainty of these coordinates was smaller than 2 mm.

The first step in the RTK processing to validate the success of our approach was a confirmation of the RTK positioning solutions using the data recorded at CGSJ and DRHS. In this case, although test data was recorded in static mode, the data was processed as if it was obtained in kinematic mode. CGSJ was treated as the base station and DRHS as the rover. We present the statistics for the ambiguity-fixed RTK positioning solutions between CGSJ and DRHS in Table 1.

Table 1. Summary statistics for ambiguity-fixed RTK solutions, CGSJ to DRHS.

	Mean (cm)	Std. (cm)	r.m.s. (cm)
dX	-0.1	1.1	1.1
dY	-0.2	2.3	2.3
dZ	-0.3	1.5	1.5
dN	0.5	1.4	1.5
dE	0.6	1.3	1.4
dU	0.4	2.3	2.3

Kinematic Results

Since we have validated the success of the ionosphere-nullification approach using the data recorded in static mode at CGSJ and DRHS, we further tried to confirm its validity using the data collected in kinematic mode with the onboard GPS receiver. A pair of long/short baselines (i.e., DRHS to BOAT and CGSJ to BOAT) was estimated at each epoch and used to characterize long-baseline positioning performance.

After a pair of long/short baselines was estimated at each epoch, baseline components were compared for each pair of solutions. Figure 14 illustrates that there is only a few cm variation between the long and short RTK positioning solutions. Table 2 provides the summary statistics. A few mm mean differences are observed in each Cartesian component, and the comparison 1σ noise level is at the few cm level.

Table 2. Summary statistics for differences between ambiguity fixed RTK solutions: CGSJ to BOAT and DRHS to BOAT.

	Mean (cm)	Std. (cm)	r.m.s. (cm)
dX	-0.1	0.9	0.9
dY	-0.2	1.7	1.7
dZ	-0.3	1.6	1.6

dN	-0.3	1.2	1.2
dE	-0.2	1.0	1.0
dU	-0.1	2.0	2.0

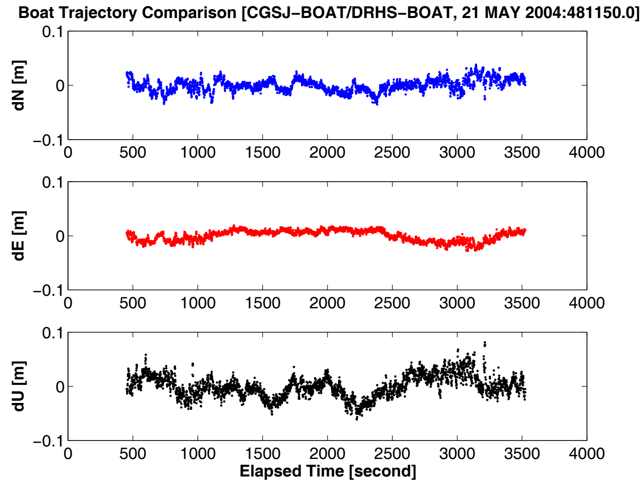

Figure 14. Difference of RTK positioning solutions, CGSJ to BOAT (short baseline) and DRHS to BOAT (long baseline) in local geodetic coordinates.

CONCLUSIONS

We have experienced a number of challenges in resolving ambiguities for longer baselines. One of the major challenges is the presence of unmodelled atmospheric (i.e., ionospheric and tropospheric) delays. In this paper, we discussed another possible approach that does not rely on the convergence of a parameter (atmospheric delay or float ambiguities), but which nullifies and estimates the effect of the differential atmospheric delay in the ambiguity search process.

We propose the ionosphere-nullification technique which can virtually eliminate the large first-order ionospheric effects using the ionosphere observable in the simultaneous ambiguity search process. We also propose the adaptive estimator for estimating the tropospheric delays.

Although this technique was originally developed for single-baseline RTK over long distances in kinematic mode, it can be considered as an alternative approach or a parallel process for network RTK when requiring extrapolation of the differential ionospheric corrections for a rover located outside the network. It can be also used in cases where the rover located inside the network is experiencing localized anomalous ionospheric delays due to severe ionospheric activity. We plan to implement this technique into our network RTK software which is currently under development.

The performance of new approach was demonstrated using data recorded at a 1 Hz data rate at a pair of base stations on either side of the Bay of Fundy in eastern Canada, the terminals of an approximately 74 km ferry route. Data was also recorded on the ferry boat itself when the boat was at or near a terminal. For both static and kinematic tests over the 74 km baseline, a few mm mean differences were observed in each Cartesian component, and the comparison 1σ noise level was at the few cm level.

ACKNOWLEDGEMENTS

The authors would like to thank the U.S. Office of Naval Research for funding some parts of the core research reported in this paper during 2003-2004 through an agreement with the University of Southern Mississippi. Other research was carried out under contract specifically for GNSS simulation system development for modeling environmental errors. The support of the Korea Astronomy and Space Science Institute is gratefully acknowledged.

REFERENCES

Bassiri, S. and G. A. Hajj, Higher-order ionospheric effects on the global positioning system observables and means of modeling them, Manuscripta Geodaetica, Vol. 18, 1993, pp. 280-289.

Beutler, G., GPS satellite orbits, in GPS for Geodesy, 2nd edition, edited by P. J. G. Teunissen and A. Kleusberg, Chapter 2, pp. 43-110, Spring-Verlag, New York, 1998.

Brunner, F. K. and W. M. Welsch, Effect of the troposphere on GPS measurements, GPS World, Vol. 4, No. 1, January 1993, pp. 42-51.

Chen, G. and T. A. Herring, Effects of atmospheric azimuthal asymmetry on the analysis of space geodetic data, Journal of Geophysical Research, Vol. 102, No. B9, 1997, pp. 20489-20502.

Collins, J. P. and R. B. Langley, Estimating the Residual tropospheric delay for airborne differential GPS positioning, Proceedings of ION GPS-97, Kansas City, MO, 16-19 September 1997, pp. 1197-1206.

Davis, J. L., T. A. Herring, I. I. Shapiro, A. E. E. Rogers, and G. Elgered, Geodesy by radio interferometry: Effects of atmospheric modelling errors on estimates of baseline length, Radio Science, Vol. 20, No. 6, 1985, pp. 1593-1607.

Euler, H.-J. and H. Landau, Fast GPS ambiguity resolution on-the-fly for real-time application, Proceedings of 6th International Geodetic Symposium on Satellite Positioning, Columbus, Ohio, 17-20 March 1992, pp. 650-659.

Fotopoulos, G. and M. E. Cannon, An overview of multiple-reference station methods for cm-level positioning, GPS Solutions, Vol. 4, No. 3, January 2001, pp. 1-10.

Ghoddousi-Fard, R. and P. Dare, Comparing various GPS neutral atmospheric delay mitigation strategies: A high latitude experiment, Proceedings of ION GNSS 2006, Fort Worth, Texas, 25-28 September 2006, pp. 1945-1953.

Gregorius, T. and G. Blewitt, The effect of weather fronts on GPS measurements, GPS World, Vol. 9, No. 5, May 1998, pp. 52-60.

Herring, T. A., Modeling atmospheric delays in the analysis of space geodetic data, Proceedings of Refraction of Transatmospheric Signals in Geodesy, Netherlands Geodetic Commission Series, Vol. 36, 1992, pp. 157–164.

Hoque, M. M. and N. Jakowski, Higher order ionospheric effects in precise GNSS positioning, Journal of Geodesy, Vol. 81, No. 4, 2007, pp. 259-268.

Hugentobler, U., S. Schaer and P. Fridez, Bernese GPS software version 4.2, Astronomical Institute, University of Berne, Switzerland, 2001.

IGS GFZ, Figures and Statistics for Broadcast Orbits wrt IGS Rapid Orbits, The IGS Analysis Center Coordinator at GFZ Potsdam. [Online] 18 September 2007. <http://www.gfz-potsdam.de/pb1/igsacc/igsacc_BRDC.html>

Kashani, I., D. Grejner-Brzezinska and P. Wielgosz, Towards instantaneous RTK GPS over 100 km distances, Proceedings of ION 60th Annual Meeting, Dayton, Ohio, 7-9 June 2004, pp. 679-685.

Kim, D., S. Bisnath, R. B. Langley and P. Dare, Performance of long-baseline real-time kinematic applications by improving tropospheric delay modeling, Proceedings of ION GNSS 2004, Long Beach, California, 21-24 September 2004, pp. 1414-1422.

Kim, D. and R. B. Langley, Nullification of differential ionospheric delay for long-baseline real-time kinematic applications, Proceedings of ION 61st Annual Meeting, Cambridge, Massachusetts, 27-29 June 2005, pp. 949-960.

Landau, H., U. Vollath and X. Chen, Virtual reference station systems, Journal of Global Positioning Systems, Vol. 1, No. 2, 2002, pp. 137-143.

Langely, R. B., GPS, the ionosphere, and the solar maximum, GPS World, Vol. 11, No. 7, July 2000, pp. 44-49.

Lawrence, D., R. B. Langley, D. Kim, F.-C. Chan and B. Pervan, Decorrelation of troposphere across short baselines, Proceedings of IEEE/ION PLANS 2006, San Diego, California, 24-27 April 2006, pp. 94-102.

McCarthy, D. D. and G. Petit, International Earth Rotation Service Conventions 2003, IERS Technical Note No. 32. [Online] 18 September 2007. <http://www.iers.org/iers/publications/tn/tn32/tn32.pdf>.

Niell, A. E., Global mapping functions for the atmospheric delay at radio wavelengths, Journal of Geophysical Research, Vol. 101, No. B2, 1996, pp. 3227–3246.

Niell, A. E., A. J. Coster, F. S. Solheim, V. B. Mendes, P. C. Toor, R. B. Langley and C. A. Upham, Comparison of measurements of atmospheric wet delay by radiosonde, water vapor radiometer, GPS, and VLBI, Journal of Atmospheric and Oceanic Technology, Vol. 18, No. 6, June 2001, pp. 830–850.

Petrovski, I., S. Kawaguchi, H. Torimoto, B. Townsend, S. Hatsumoto and K. Fuji, An impact of high ionospheric activity on MultiRef RTK network performance in Japan, Proceedings of ION GPS-2002, Portland, Oregon, 24-27 September 2002, pp. 2247-2255.

Rizos, C., Network RTK research and implementation - A geodetic perspective, Journal of Global Positioning Systems, Vol.1, No.2, 2002, pp. 144-150.

Rocken, C., T. Van Hove, J. Johnson, F. Solheim and R. Ware, GPS/STORM – GPS sensing of atmospheric water vapour for meteorology, Journal of Atmospheric and Oceanic Technology, Vol. 12, 1995, pp. 468-478.

Saastamoinen, J., Atmospheric correction for the troposphere and stratosphere in radio ranging of satellites, Geophysical Monograph, Vol. 15, 1972, pp. 247–251.

Skidmore, T. and F. Van Graas, An investigation of tropospheric errors on differential GNSS accuracy and integrity, Proceedings of ION GNSS 2004, Long Beach, California, 21-24 September 2004, pp. 2752-2760.

Teunissen, P. J. G., The least-squares ambiguity decorrelation adjustment: A method for fast GPS integer ambiguity estimation, Journal of Geodesy, Vol. 70, No. 1-2, November 1995, pp. 65-82.

UNB GGE, GPS broadcast orbit accuracy statistics compared with IGS orbit, The University of New Brunswick, Department of Geodesy and Geomatics Engineering, GPS Lab. [Online] 18 September 2007. <http://gge.unb.ca/gauss/htdocs/grads/orbit/>

Wielgosz, P., I. Kashani and D. Grejner-Brzezinska, Analysis of long-range network RTK during a severe ionospheric storm, Journal of Geodesy, Vol. 79, No. 9, December 2005, pp. 524-531.

Wubbena, G., A. Bagge and M. Schmitz, RTK Networks based on Geo++® GNSMART - Concepts, implementation, results, Proceedings of ION GPS 2001, Salt Lake City, Utah, 11-14 September 2001, pp. 368-378.

Ziebart, M., P. Cross and S. Adhya, Modeling photon pressure: The key to high-precision GPS satellite orbits, GPS World, Vol. 13, No. 1, January 2002, pp. 43-50.